CrystEngComm

Reversible Synthesis of Structured MOF-to-Metal Oxide Nanorods

Journal:	*CrystEngComm*
Manuscript ID	CE-COM-07-2022-000969.R1
Article Type:	Communication
Date Submitted by the Author:	18-Aug-2022
Complete List of Authors:	Joshi, Jayraj; Georgia Institute of Technology, Chemical & Biomolecular Engineering Moran, Colton; Georgia Institute of Technology, Chemical & Biomolecular Engineering Feininger, Harold; Georgia Institute of Technology, Chemical & Biomolecular Engineering Walton, Krista; Georgia Institute of Technology, Chemical & Biomolecular Engineering

COMMUNICATION

Received 00th January 20xx,
Accepted 00th January 20xx

DOI: 10.1039/x0xx00000x

Reversible Synthesis of Structured MOF-to-Metal Oxide Nanorods

Jayraj N. Joshi,[a‡] Colton M. Moran,[a‡] Harold P. Feininger,[a] and Krista S. Walton*[a]

Aluminum framework MIL-53(Al) acquires uniform, one-dimensional crystal growth when produced from insoluble metal sources. Pyrolysis of this structured MIL-53(Al) forms new alumina-based nanorods that extend up to 5µm in one dimension without external templates or structure-direction and serve as growth templates for regenerative MOF production.

Nanoscale structural control has experienced decades of interest in the scientific community.[1] Particularly in catalysis and adsorption applications, textural property control (e.g. pore size distribution, accessibility, and surface chemistry) over employed porous substrates and composites directly dictates process performance and applicability.[2-4] Similarly, one-dimensional structural control has yielded significant enhancements in material development related to optics and electronics.[5-9] Ideally, methods for enacting geometry, pore chemistry, and structure control over commonly employed porous substrates such as metal oxides can generate broad impacts in materials science. The extensive library of exotic microstructures provided by metal-organic frameworks (MOFs) lends strong potential to transition many unique architectures to derived metal oxide-based composites across the periodic table. Previous reports discuss the "structural memory" of MOF-derived oxide formation—selecting framework precursors of desirable metal composition and morphology easily transfers MOF structures onto resulting metal oxides/carbonaceous materials.[10-12] Benefits of utilizing MOFs derived from insoluble metal precursors, such as metals, carbides, and hydroxides, are not as prevalent in literature however. Frameworks created from such media adapt unconventional morphologies, and are easily patterned and positioned onto substrates without the use of modulation or structure-directing methods.[13, 14] Scientists may consequently generate and transfer a host of new structural templates onto metal oxide-based materials, while simultaneously positioning them on hierarchical supporting substrates. Here, we extend the application of the subset "insoluble metal precursor-synthesized MOFs" to their derived oxides. Highly accessible aluminum oxide microstructures are developed from our previously reported Al_4C_3-derived MIL-53(Al),[15] which exhibits self-supported microneedle structures. The newly produced metal oxide composite allows for new applications in the field of both MOF chemistry and conventional catalysis/adsorption processes common for metal oxide composites—both of which are discussed here.

Previously reported aluminum carbide and metallic aluminum sources for structured MIL-53(Al) formation were utilized as growth precursors.[14, 15] In contrast to conventionally synthesized MIL-53(Al), these crystallites extend perpendicularly from the underlying insoluble metal precursors, forming a densely-packed monolayer of crystalline microneedles. Figure 1 illustrates the synthesis of converting insoluble aluminum-based media to MIL-53(Al), and then into nanorod-shaped Al_2O_3 composite media. MIL-53(Al) thermally degrades at temperatures >400°C in inert atmospheres.[16] Accordingly,

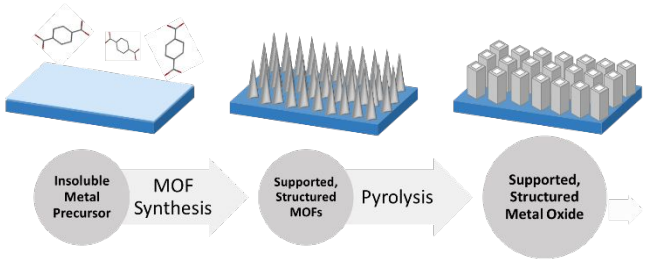

Figure 1. Schematic of metal organic framework (middle) and subsequent *MIL-53(Al)-oxide* (right) formation using insoluble metal precursors (left). Dark blue rectangle represents the insoluble metal precursor, where the lighter blue region is intended to illustrate the uppermost monolayer in which structure formation occurs. Grey geometries represent the MOF and resultant oxide-based composite.

[a] *School of Chemical &Biomolecular Engineering, Georgia Institute of Technology, 311 Ferst Dr. NW, Atlanta, GA 30332 USA*

Electronic Supplementary Information (ESI) available: [details of any supplementary information available should be included here]. See DOI: 10.1039/x0xx00000x

MOF precursors were pyrolyzed at 600°C (see SI for further details) to destroy the framework and produce a MIL-53(Al)-derived aluminum oxide-based composite. The composite material obtained from pyrolysis of Al_4C_3-derived MIL-53(Al) is named *MIL-53(Al)-oxide* in this report hereafter for brevity. It should be noted that a templating procedure was not utilized in either step; the one-directional growth inherent of using the insoluble precursor is passed down to the MOF, and then *MIL-53(Al)-oxide*.

Before and after pyrolysis images of the porous materials are depicted in Figure 2. MIL-53(Al) precursors grown on Al_4C_3 and aluminum foil are shown for reference in Figures 2a and b, respectively. MIL-53(Al) microneedles transform into porous nanotubes after pyrolysis. Figures 2**c** & d reveal the formation of elongated, rod-like particles in *MIL-53(Al)-oxide*. Supplementary Figures S1 & S2 show the same result for pyrolyzed MIL-53(Al) grown on and from aluminum alloy mesh. EDS data in Figure S2 reveals the existence of a carbonaceous surface dispersed throughout the mesh-based composite. Carbon deposition is expected from previous MOF degradation studies in inert environments, and results from the pyrolysis of terephthalate linkers.[11] Needle apexes of the MOF precursor truncate after pyrolysis, suggesting they were composed primarily of terephthalate molecules in MIL-53(Al). The orientation of the alumina rods on *MIL-53(Al)-oxide* suggests that the one-dimensional aluminum oxide backbone of MIL-53(Al) extending along the *a* axis grows perpendicular to the insoluble precursor surface. Evolved aluminum oxide-based nanorods showcasing the same orientation accordingly exhibit the "structure memory" presented in Figure 1 that is uniquely afforded by MOF-derived oxide/carbon production.

Large square-shaped openings of approximately 220nm are positioned at the outer ends of the tubular structures. The large central cavity in Figure 2d appears to penetrate downwards through the tube and connect the inner free space. Li and coworkers remarked that a lack of order and interconnectivity is a frequent limitation of MOF-derived porous media.[10] Therefore, this observation constitutes an important advancement in migrating the order and connectivity of MOFs to their respective derived composites, in addition to morphology. Distinguishable ridge-like features and openings along the sides of the nanorods in Figures 2c and d indicate a heterogeneous pore structure, which is characterized later in this report through porosity measurements. Figure 2e generalizes the dimensionality of *MIL-53(Al)-oxide*, where nanorods extend a few microns from the underlying surface, and retain uniform shape and size across studied particle aggregates. Framework destruction results in a 78% decrease of accessible BET surface area and 44% decrease in total measured pore volume (Figure 2f). This is due to the evacuation of bridging framework ligands that generate large adsorption surfaces throughout the MIL-53(Al) precursor. The residual BET surface area of 250.9 m^2 g^{-1} shows *MIL-53(Al)-oxide* still possesses microporosity on the upper-end of what is typically observed for alumina-based materials, while maintaining a broad spectrum of pore sizes.[17-20] A mass loss of 61% is observed after pyrolysis, which agrees well with the reported 64% mass loss from TGA data of Al_4C_3-derived MIL-53(Al) in an inert atmosphere.

Many reports exist for the structured growth of aluminum oxide. MOF-derived oxide templating methods however offer a uniform synthesis methodology for creating these materials, as the same general steps can be taken to produce carbon/metal oxide-based materials for a variety of frameworks that may possess similar morphologies. Yamauchi and coworkers exemplify this in their development of similar fibular structures through carbonizing Al-PCP rod-shaped crystals.[11] However, the templated nature of the composite presented here enables unique material modification opportunities. Two possible applications of *MIL-53(Al)-oxide* presented here exemplify the possible uses of MOF-derived oxides from insoluble precursors: (1) MOFs can be regrown onto derived-oxide structures, and (2) mixed-metal oxide composites can be generated by manipulation of the MOF precursor.

MOF repair and regrowth strategies can generate interesting material property solutions. For instance, the SACRed procedure for healing ZIF-8 crystals by Nair and coworkers[21] was hypothesized to possibly enhance the lifetime of ZIF-based filtration and membrane media employed in corrosive environments. Multiple MOF growth cycles were also employed to create stable and selective catalyst media, by

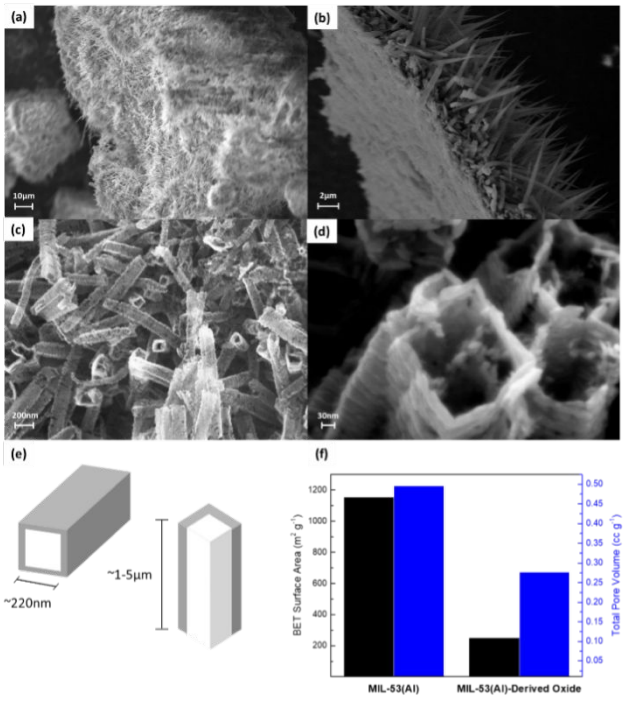

Figure 2. Characterization of *MIL-53(Al)-oxide*. SEM images of MIL-53(Al) precursor derived from (a) aluminum carbide (Al_4C_3) and (b) metallic aluminum (foil) are presented for reference, (c-d) shows derived alumina-based nanorod structures from pyrolysis of Al_4C_3-derived MIL-53(Al), (e) cartoon depicting average dimensions of evolved nanorod structures, (f) changes in porosity from Al_4C_3-derived MIL-53(Al) precursor and subsequent *MIL-53(Al)-oxide*, calculated from N_2 physisorption data at 77K.

"sandwiching" encapsulated active sites between framework layers.[22, 23] Through such studies, one can envision simple processes to recycle MOF materials and significantly extend their usable lifetimes, or add further complexity to MOF-based products, in a facile and stepwise manner.

Structured aluminum oxide tubes examined on *MIL-53(Al)-oxide* uniquely serve as a scaffold and aluminum metal center source for MIL-53(Al) regrowth. The regenerability of MIL-53(Al) was demonstrated by repeating two steps (1) thermal degradation of Al_4C_3-derived MIL-53(Al) to produce *MIL-53(Al)-oxide*, and (2) regrowth of MIL-53(Al) on and from *MIL-53(Al)-oxide* via hydrothermal reaction. The reaction used for MIL-53(Al) regrowth is the same used to make the original Al_4C_3-derived MIL-53(Al) precursor, but assumes the derived oxide has the stoichiometry of Al_2O_3 to determine linker and DI water amounts (further description in SI). A general scheme of cyclic MOF production is presented in Figure 3a. MIL-53(Al) growth was cycled twice in succession, where resulting products are named Cycle 1 and Cycle 2, respectively. Micrographs in Figure S3 provide evidence of reformed MIL-53(Al) crystals after one and two pyrolysis-growth cycles. Regenerated microneedles in Cycles 1 and 2 are uniform in appearance with each other and the original Al_4C_3-derived MIL-53(Al). Impressively, N_2 physisorption measurements at 77K (Figure 3b) show the Cycle 1 and Cycle 2 completely recover porosity. BET surface areas

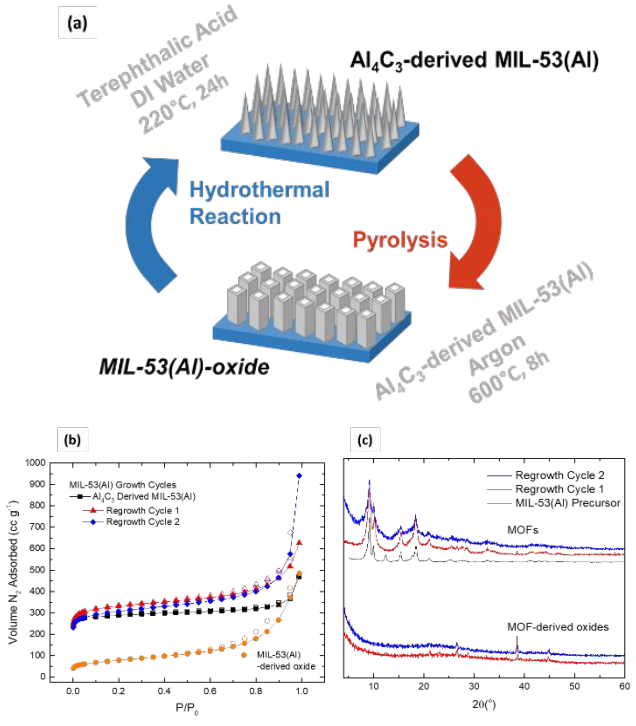

Figure 3. Characterization of MIL-53(Al) growth cycle products and derived oxides. (a) Scheme of growth cycle reactions, (b) N_2 physisorption at 77K, and (c) powder X-ray diffraction measurements of regeneration cycle materials.

derived from the N_2 adsorption data in Table S1 are likewise consistent for regenerated MOFs amongst each regrowth cycle and with Al_4C_3-derived MIL-53(Al). A modest increase in surface area is even observed, which may be attributed to accumulation of microporous materials between pyrolysis runs. In addition, mesopores in regenerated MIL-53(Al) samples are qualitatively apparent by capillary condensation behavior in N_2 adsorption curve slopes in Figure 3b, as compared to the strictly microporous original MIL-53(Al) precursor, and quantified by increased pore volumes for Cycles 1 and 2 in Table S1.[24] Residual mesoporous structures from *MIL-53(Al)-oxide* growth precursors manifest in regenerated MOFs, uniquely instilling mesoporosity in resulting composites. PXRD data in Figure 3c confirm reappearance of the MIL-53(Al) crystal phase for Cycle 1 and Cycle 2. Crystalline microstrain is clearly visible in the patterns for the regenerated products. Because MOF growth localizes on alumina nanorods, ligand accessibility and coordination hindrance from particle aggregation and surface heterogeneity likely introduce lattice strain in the final products. Diffraction measurements show the existence of pyrolytic carbon (JCPDF no. 01-083-6084) and aluminum (JCPDF no. 00-001-1180), but do not reveal any long-range order for the aluminum oxide structures. The Al_2O_3 phase is subsequently assumed to be amorphous, as was seen through previous thermogravimetry measurements on MIL-53(Al) prepared from insoluble metal precursors.[25]

Several MOF regeneration reports already exist in the literature. Earlier investigations on MOF-5 and HKUST-1 by Han and Lah[26] also recover the porosity of their original frameworks after regeneration, as seen for MIL-53(Al) here. Several critical differences are noted here however. Hazardous acidic and/or alkaline modulators used in previous MOF regrowth literature are not necessary for the multiple MIL-53(Al) growth cycles shown here. More importantly however, because architectures are supporting these materials, the spatial positions of microneedles and rods are affixed when cycling between MIL-53(Al) and *MIL-53(Al)-oxide*, respectively. In contrast, previous reports only examine non-supported MOF regrowth. This allows framework regrowth to be localized on the same oxide nanorods formed from original MIL-53(Al) growth from insoluble metal precursors. Truly invariable MOF regeneration results, where microneedles are forced to reconstruct on the same locations from which they were destroyed during pyrolysis. Memory of growth location is inherently not possible with non-supported MOF growth techniques but is attained here without structure direction or templates during regrowth cycles. This allows the progression of MOF recycling to MOF-based composites, devices, and hierarchical media, where spatial growth is consistent between cycles. By extension, this methodology allows the generation of consistent and homogeneous porous structures.

Hydrogen sulfide (H_2S) is a pervasive contaminant in many fuel streams.[27] The vapor is oftentimes encountered at low concentrations (< 1%), but still complicates processes due to its high toxicity and corrosive nature.[28, 29] Development of H_2S scavengers which function effectively at low gas concentrations can greatly facilitate energy-related remediation operations.

Methods of leveraging the well-known chemical degradation of H_2S over inexpensive iron oxide (Fe_2O_3) are explored in literature, and the oxide is commonly integrated into commercial desulfurization media.[30] Moreover, adsorption-based H_2S removal can offer a simpler and more cost-effective method than common amine-based scrubbing technologies.[30, 31] As with other catalyst/adsorbent-support composites, the efficient integration of iron oxide chemisorbents can form H_2S-removal products capable of high active site accessibility while stabilizing the Fe_2O_3-impregnate particles.

Accordingly, iron oxide composites were formed with the *MIL-53(Al)-oxide*. Al_4C_3-derived MIL-53(Al) was first utilized as the precursor for impregnation and subsequently pyrolyzed (sample preparation is detailed in the Supplementary Information). The hierarchical pore structure of impregnated *MIL-53(Al)-oxide* is characterized by pore size distributions in Figure 4. Well-defined micropores between 10-13Å are apparent for parent and impregnated *MIL-53(Al)-oxide*. In addition to the 220nm macropore in *MIL-53(Al)-oxide* discovered via electron imaging, N_2 data reveals an array of mesopores ranging from under 5nm to around 30nm. The mixture of macropores, mesopores, and micropores together is rare; Bruce and coworkers only developed the first reported material (an α-MnO_2 solid) to display such behavior in 2013, and not many more have been reported thereafter.[32, 33] For aluminum oxides specifically, meso- and micropores are typically only observed for γ-Al_2O_3 phases, and bimodal macroporous-mesoporous aluminas require surfactants and/or growth templates.[34, 35] MOF-derived oxides easily achieve these qualities however, as Mounfield III et al. also noticed similar attributes in MIL-125(Ti)-derived titania.[36] Multimodal pore systems are highly desirable in applications dictated by mass transfer limitations, sieving effects, or material accessibility issues. These textural insights highlight the novelty and intricacy of *MIL-53(Al)-oxide* and other structure MOF-derived oxides. Pore accessibility unsurprisingly decreases after impregnation. Microporosity is largely retained, but mesopores from 10-20nm become absent. These differences may result from the iron oxide aggregates simply occupying larger pore spaces. The impregnate can additionally change how MIL-53(Al) pyrolyzes—minimizing the propagation of certain mesopores throughout the substrate. Decorated pores along the sides of the MIL-53(Al)-oxide tubes, as discussed in Figure 2c facilitate guest molecule accessibility throughout the bulk. SEM micrographs in Figure S4 confirm the morphology of the impregnated samples is consistent with unmodified *MIL-53(Al)-oxide* presented in Figure 2.

Humid hydrogen sulfide exposures were conducted on *MIL-53(Al)-oxide* both with and without iron oxide impregnation (see Supplementary Information for experimental details). SEM-EDS measurements of the iron-oxide impregnated composite in Figure 5a validate even dispersion of iron across the sample. Average weight percent of iron and aluminum from EDS data is 15.4% and 28.4%, respectively. Sulfur is also detected fairly homogeneously across the particle surfaces. This distribution is likely a result of the large iron oxide loading and dispersion across the sample, supplying numerous adsorption sites for H_2S. High resolution S2p XPS data in Figure S5 confirms the reactive degradation of H_2S over iron oxide. Species around 168-170eV correspond well with iron sulfates ($FeSO_4$, $Fe_2(SO4)_3$) formed via oxidation of H_2S.[37] A small presence of iron(II) sulfite is detected at 162eV, while significant detection of elemental sulfur (S_8) in $S2p_{3/2}$, $S2p_{1/2}$ scans at 164eV is consistent with H_2S decomposition over iron oxides.[37, 38] Figure S6 provides a $Fe2p_{1/2}$ information from 724eV-726eV and a $Fe2p_{3/2}$ peak at 711eV supporting the existence of iron sulfates, as observed in the sulfur scan in Figure S5.[37] Existence of non-converted iron oxide(s) in $Fe2p_{1/2}$ measurements around 720eV may suggest some amount of the iron oxide surfaces were inaccessible to H_2S, or simply arise from oxide detection underneath the sulfated monolayer. It should be noted the elemental mapping and XPS information may not be representative of the bulk distribution due to depth resolution limitations.

Variance in desulfurization performance across evaluated iron oxide impregnated MOF-derived alumina composites become apparent however after determining iron and sulfur loadings via ICP-OES. Figure 5b illustrates repeatable iron loadings across the various batches of impregnated *MIL-53(Al)-oxide*. ICP and previously mentioned EDS data both estimate average iron loadings of around 15 wt% among investigated samples. This is expected, as impregnate amounts are restricted by available substrate pore volume in the incipient wetness method, which is uniform in the highly ordered Al_4C_3-derived MIL-53(Al) precursor. Sulfur loadings on the non-impregnated sample range from 0.93-1 mmol S g^{-1}. Sulfur loadings are conversely quite different among the four iron oxide impregnated *MIL-53(Al)-oxide* batches. One of the tested samples even has a lower sulfur uptake than the non-impregnated control sample. Figure 5b clearly demonstrates that H_2S degradation is not a function of iron oxide loading. It is more likely dictated by the relative accessibility of the iron oxide active sites sample-to-sample. Homogenous distribution and size of iron oxide aggregates is not controllable across batches through impregnation. So, the relative difference in accessibility

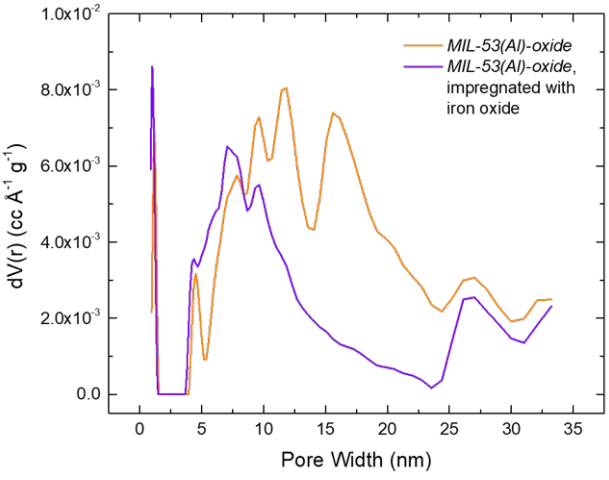

Figure 4. Pore size distributions from N_2 measurements at 77K for unmodified and impregnated *MIL-53(Al)-oxide*.

of iron oxide adsorption sites likely caused the disparity in sulfur uptake. Still, the apparent sulfur activity of the composite shows the propensity to easily produce materials with highly accessible chemical reaction sites through this mixed metal oxide production scheme.

Analysis of impregnated *MIL-53(Al)-oxide* illustrates a facile methodology of imbuing heterogeneous surface chemistry into aluminum oxide support structures. High impregnate infiltrations are achievable by loading the MOF precursor instead of the aluminum oxide support directly—taking advantage of the markedly greater pore volume inherent of MOFs. Furthermore, composites integrate directly onto supported structures without further modification when insoluble metal precursors are used for MOF growth. As a result, this method may be extended to any desired impregnate species for loading onto alumina support

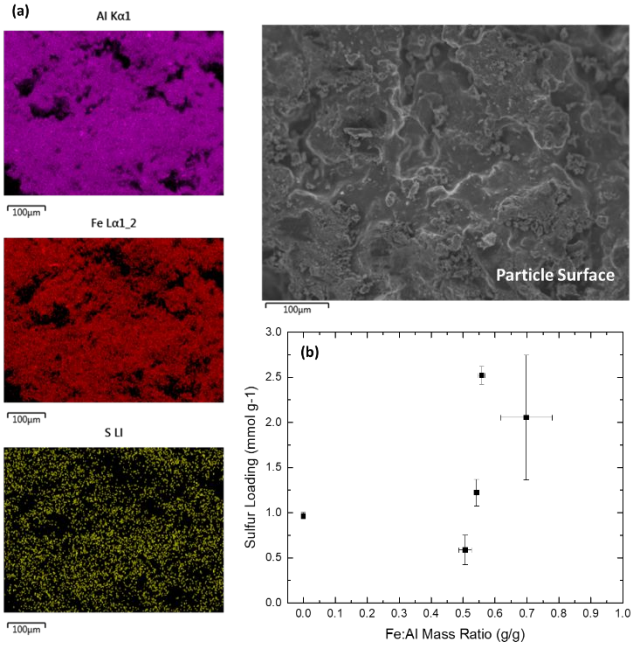

Figure 5. Elemental analysis of iron oxide-impregnated *MIL-53(Al) oxide* following H_2S exposure. (a) SEM-EDS mapping of aluminum, iron, and sulfur across particle surface and (b) sulfur loadings on unmodified and impregnated *MIL-53(Al)*, as determined by ICP-OES.

Conclusions

This report demonstrates the facile construction of *MIL-53(Al)-oxide*: a supported composite containing self-oriented aluminum oxide-based nanorods. Importantly, the structure was transitioned from MIL-53(Al), which naturally acquires one-dimensional crystal growth when produced from insoluble metal precursors—not afforded by conventional synthesis. Derived nanorods retain growth orientation, relative size dimensions, and support structure (carbonized Al_4C_3, metallic aluminum, Al_2O_3, etc.) from which the MIL-53(Al) precursor was grown. Produced architectures display a wide range of macro, meso, and micropores, and acquire new material characteristics that enable several interesting uses.

The supported nature of *MIL-53(Al)*-oxide instilled unique capabilities for MOF regeneration. MIL-53(Al) microneedles were regrown twice from *MIL-53(Al)-oxide* with full recovery of porosity. Spatial regrowth control that is not possible in previous regrowth strategies using non-supported MOFs is demonstrated here for the first time. This control is due to insoluble metal precursor supporting structures, which support the alumina-based nanorods that serve as regrowth templates between multiple MOF growth cycles. Additionally, mixed-metal oxide synthesis was explored through pretreatment of the MIL-53(Al) precursor. Accessible and well-dispersed iron oxide was easily attained, where Fe_2O_3 active sites displayed reactivity with hydrogen sulfide at low concentrations. This result affirms the applicability of the MOF-derived composite as potential support media for impregnate-based adsorption/catalysis media. Although these applications have been explored similarly in prior work, the unique MOF-derived composite here affords unique advances in material control for both cases. This hierarchical support structure manufacturing strategy can enable construction of a platform towards integrating Al_2O_3 media onto devices, monoliths, membranes, and other media relevant to catalysis and separations.

Author Contributions

The manuscript was written through contributions of all authors. All authors have given approval to the final version of the manuscript. ‡These authors contributed equally.

Conflicts of interest

There are no conflicts to declare.

Acknowledgments

This work is supported by the Center for Understanding and Control of Acid Gas-Induced Evolution of Materials for Energy (UNCAGE-ME), an Energy Frontier Research Center funded by U.S. Department of Energy (US DOE), Office of Science, Basic Energy Sciences (BES) under Award no. DE-SC0012577

Notes and references

1. S. Iijima, *nature*, 1991, **354**, 56-58.
2. D. Trimm and A. Stanislaus, *Applied Catalysis*, 1986, **21**, 215-238.
3. A. Taguchi and F. Schüth, *Microporous and mesoporous materials*, 2005, **77**, 1-45.
4. A. Corma, *Chemical reviews*, 1997, **97**, 2373-2420.
5. X. Wang and G.-R. Han, *Microelectronic Engineering*, 2003, **66**, 166-170.
6. M. S. Gudiksen, L. J. Lauhon, J. Wang, D. C. Smith and C. M. Lieber, *nature*, 2002, **415**, 617-620.
7. L. J. Lauhon, M. S. Gudiksen, D. Wang and C. M. Lieber, *nature*, 2002, **420**, 57-61.
8. H. Dai, *Surface Science*, 2002, **500**, 218-241.
9. C. R. Martin, *Science*, 1994, **266**, 1961-1966.

10. K. Shen, X. Chen, J. Chen and Y. Li, *Acs Catalysis*, 2016, **6**, 5887-5903.
11. R. R. Salunkhe, J. Tang, Y. Kamachi, T. Nakato, J. H. Kim and Y. Yamauchi, *ACS nano*, 2015, **9**, 6288-6296.
12. Y. V. Kaneti, J. Tang, R. R. Salunkhe, X. Jiang, A. Yu, K. C. W. Wu and Y. Yamauchi, *Advanced materials*, 2017, **29**, 1604898.
13. G. Zhan and H. C. Zeng, *Chemical Communications*, 2017, **53**, 72-81.
14. J. Kim, S. Lee, J. Kim and D. Lee, *Advanced Functional Materials*, 2019, **29**, 1808466.
15. C. M. Moran, J. N. Joshi, R. M. Marti, S. E. Hayes and K. S. Walton, *Journal of the American Chemical Society*, 2018, **140**, 9148-9153.
16. D. V. Patil, P. B. S. Rallapalli, G. P. Dangi, R. J. Tayade, R. S. Somani and H. C. Bajaj, *Industrial & engineering chemistry research*, 2011, **50**, 10516-10524.
17. H. Pines and W. O. Haag, *Journal of the American Chemical Society*, 1960, **82**, 2471-2483.
18. S. M. Morris, P. F. Fulvio and M. Jaroniec, *Journal of the American Chemical Society*, 2008, **130**, 15210-15216.
19. S. Zhang, Y. Wang, Y. Tan, J. Zhu, K. Liu and J. Zhu, *Materials Research Express*, 2016, **3**, 074004.
20. S. Goldberg, I. Lebron, D. L. Suarez and Z. R. Hinedi, *Soil Science Society of America Journal*, 2001, **65**, 78-86.
21. K. C. Jayachandrababu, S. Bhattacharyya, Y. Chiang, D. S. Sholl and S. Nair, *ACS applied materials & interfaces*, 2017, **9**, 34597-34602.
22. M. Zhao, K. Yuan, Y. Wang, G. Li, J. Guo, L. Gu, W. Hu, H. Zhao and Z. Tang, *Nature*, 2016, **539**, 76-80.
23. F. Huo, *Science Bulletin*, 2016, **61**, 1726-1727.
24. J. Rouquerol, D. Avnir, C. Fairbridge, D. Everett, J. Haynes, N. Pernicone, J. Ramsay, K. Sing and K. Unger, *Pure and applied chemistry*, 1994, **66**, 1739-1758.
25. Y. Zhang, Q. Gao, Z. Lin, T. Zhang, J. Xu, Y. Tan, W. Tian and L. Jiang, *Scientific reports*, 2014, **4**, 1-6.
26. S. Han and M. S. Lah, *Crystal Growth & Design*, 2015, **15**, 5568-5572.
27. F. S. Manning and R. E. Thompson, *Oilfield processing of petroleum: natural gas*, Pennwell books, 1991.
28. R. Reiffenstein, W. C. Hulbert and S. H. Roth, *Annual review of pharmacology and toxicology*, 1992, **32**, 109-134.
29. P. A. Hessel, F. A. Herbert, L. S. Melenka, K. Yoshida and M. Nakaza, *American journal of industrial medicine*, 1997, **31**, 554-557.
30. N. Abatzoglou and S. Boivin, *Biofuels, Bioproducts and Biorefining*, 2009, **3**, 42-71.
31. X. Wang, X. Ma, X. Xu, L. Sun and C. Song, *Topics in catalysis*, 2008, **49**, 108-117.
32. Y. Ren, Z. Ma, R. E. Morris, Z. Liu, F. Jiao, S. Dai and P. G. Bruce, *Nature communications*, 2013, **4**, 1-7.
33. W. Zhou, G. Tong, D. Wang, B. Zhu, Y. Ren, M. Butler, E. Pelan, D. Yan, X. Zhu and S. D. Stoyanov, *small*, 2016, **12**, 1797-1805.
34. S. J. Wilson and M. H. Stacey, *Journal of Colloid and Interface Science*, 1981, **82**, 507-517.
35. Z.-Y. Yuan, T.-Z. Ren, A. Azioune, J.-J. Pireaux and B.-L. Su, *Chemistry of materials*, 2006, **18**, 1753-1767.
36. W. P. Mounfield III, U. Tumuluri, Y. Jiao, M. Li, S. Dai, Z. Wu and K. S. Walton, *Microporous and Mesoporous Materials*, 2016, **227**, 65-75.
37. M. Descostes, F. Mercier, N. Thromat, C. Beaucaire and M. Gautier-Soyer, *Applied Surface Science*, 2000, **165**, 288-302.
38. G. Huang, E. He, Z. Wang, H. Fan, J. Shangguan, E. Croiset and Z. Chen, *Industrial & Engineering Chemistry Research*, 2015, **54**, 8469-8478.